Recovery of the intrinsic thermoelectric properties of $CaMn_{0.98}Nb_{0.02}O_3$ in 2-terminal geometry using Ag infiltration

D. Boldrin[a,], P. Boldrin[b], E. Ruiz-Trejo[b] and L. F. Cohen[a]*

[a] Department of Physics, Imperial College London, London, SW7 2AZ, UK
[*] Corresponding author, E-mail: d.boldrin@imperial.ac.uk
[b] Department of Earth Science and Engineering, Imperial College London, London, SW7 2AZ, UK

Keywords: thermoelectrics, electrical properties, oxides, ceramics

Oxide based thermoelectric (TE) materials offer several advantages over currently used intermetallic alloys due to their chemical and thermal stability at high temperatures, non-toxic elements, low cost and ease of manufacture. However, incorporation of oxides into thermoelectric generators (TEGs) is hindered by factors such as the requirement for polycrystalline materials over single crystals and the large electrode/ceramic contact resistances. The latter significantly limits the performance efficiency of a working TEG. Here we report the TE properties of Ag infiltrated polycrystalline $CaMn_{0.98}Nb_{0.02}O_3$ ceramics. We demonstrate that by using this route the intrinsic TE properties of this material are fully recovered in 2-terminal geometry through Ag infiltration, thereby overcoming the electrode TEG contact problem. This synthetic route provides opportunities for bridging the performance gap between the intrinsic TE and TEG device properties of oxides.

1. Introduction

Industrial processes generate significant quantities of waste heat which if recovered would present an important contribution towards a sustainable energy bill. Thermoelectric (TE) materials enable the direct conversion of heat into electric power and have the advantage that they require no moving parts. Prospective TE materials require a large figure-of-merit, *ZT*, to maximize conversion efficiency, but must also possess certain other mechanical and structural properties such that they can be used within a thermoelectric generator (TEG). The majority of research currently focusses on developing new functional materials with improved *ZT*. Thus far, materials have been found with $ZT > 2$ at both room and high temperature, which is

large enough to be considered competitive with other power generation systems.[1, 2] However, incorporating these materials into a TEG, which are constructed from multiple modules, is a non-trivial challenge. Designs must overcome various problems, such as compatibility between modules, stresses from the necessary temperature gradients, thermal losses and electrical contact resistances.

Transition Metal Oxide (TMO) based TE materials are attractive due to the absence of hazardous elements, such as Bi and Pb, their chemical and structural stability at high temperatures (T > 1000K), as well as their low cost and ease of manufacture.[3] Research into these materials has shown renewed interest due to significant performance increases that can be achieved through nanostructuring and aliovalent doping.[4-9] The latter vastly improves the electrical conductivity whilst maintaining a large Seebeck coefficient, and the former reduces the thermal conductivity which is often large in oxides due to contributions from the lattice. Using these approaches ZT ~0.5 has been found at high temperatures in polycrystalline samples of doped $SrTiO_3$ [10] and $CaMnO_3$.[11] It is a performance metric approaching that of Si-Ge alloys used in commercial high temperature TEGs.[12] Moreover, when taking into account material cost oxide TEGs far outperform their intermetallic counterparts, particularly for high temeprature applications. Taken together, these criteria demand further study of oxides as TE materials.

TEGs typically contain several pairs of *p*- and *n*-type conducting modules connected in series to maximize the power output. The performance efficiency of a thermoelectric device used for comparing TEG performance relates the total energy out over the total energy in, and is defined in terms of the temperature drop across the device and the dimentionless figure of merit ZT. Based on measurements of ZT the performance efficiency can be estimated theoretically, and for high temperature operation oxides are promising.[13] [14] However, a major practical obstacle in incorporating polycrystalline oxide materials in a TEG is the large contact resistance between the metal electrode and ceramic TE module.[15-17] This can reduce measured performance efficiency compared to the theoretical maximum by up to 80% in

oxides.[18-24] Importantly, most efforts to improve the oxide/electrode contact resistance focus on the interface itself **(Figure 1a** and **1b).** These include screen printing with Ag paste,[22] forming junctions with Ag paste mixed with the constituent oxide powder,[18, 19] brazing using spark plasma sintering [21] or hot press sintering.[23] More complex architectures have also been suggested, however these require more sophisticated fabrication techniques potentially cumbersome to integrate.[25] Nonetheless, even using these approaches the performance efficiency reaches only 65% of the theoretical maximum.[20, 21] Thus finding solutions to the contact resistance problem is one of the pressing needs if oxide thermolelectrics are to have a viable future.

In this paper, we have tackled the contact resistance problem by taking a different approach, not only improving the direct interfacial electrical connectivity, but also extending the electrical connectivity into the device medium **(Figure 1c).** We investigate the role of Ag infiltration into the matrix of sintered polycrystalline samples of $CaMn_{0.98}Nb_{0.02}O_3$, in order to improve the connectivity and the contact resistance. By mixing PMMA beads with $CaMn_{0.98}Nb_{0.02}O_3$ powder, where the former subsequently decomposes during sintering, ceramic matrices are produced with up to 50% porosity. Metallic Ag is then introduced into the matrix which coats the grains of the ceramic. We find that the intrinsic thermoelectric properties of $CaMn_{0.98}Nb_{0.02}O_3$, $ZT_{300K} = 0.02$ and $ZT_{1000K} = 0.3$,[4] are fully recovered in 2-terminal geometry with Ag infiltration and between 1.5 and 3 orders of magnitude better than without Ag. These results open the possibility of significantly improving the performance of oxides in TEGs.

2. Experimental

Stoichiometric quantities of $CaCO_3$ (Sigma-Aldrich, >99%), MnO_2 (Sigma-Aldrich, >99%) and Nb_2O_5 (Sigma-Aldrich, >99.99%), calculated for a 20g theoretical yield, were thoroughly mixed by hand in a mortar and pestle. This mixture was first reacted at 1100°C and 1200°C for 12 hours each with intermediate grinding. The resulting powder was ball-milled in isopropyl alcohol and then used as a bulk batch for sintering into pellets and bars as required.

Some powder was not ball-milled and instead ground by hand to investigate differences in the resulting sintered pellets. High-density ceramic samples were prepared by pressing the powder in 8mm diameter pellets under 1 tonne pressure and sintering at 1300°C for 15h. Under such conditions relative densities of ~ 86% are achieved, however in order to achieve lower densities to study the effect of additional Ag infiltration, small portions of the bulk powder were mixed with various amounts of 6 μm diameter PMMA beads before sintering into pellets. Using this method, densities as low as 45% were achieved in sintered pellets before they became too structurally weak to measure their thermoelectric properties. For Ag infiltration, sintered pellets were soaked in molten $AgNO_3$ solution for 10 minutes and once dried any excess solid $AgNO_3$ was removed by sanding. These pellets were heated to 500°C for 5 hours to decompose the $AgNO_3$ to metallic Ag.

X-ray diffraction collected from a Bruker D2 Phaser diffractometer with Cu k_α radiation confirmed the $CaMnO_3$ phase. Relative densities and open and closed porosities were measured using the Archimedes method. SEM imaging and EDX measurements were carried out using a Phenom ProX SEM. Thermoelectric measurements were made using the thermal transport option of a Quantum Design Physical Property Measurement System (PPMS-9T). With this system, samples were either measured in 2-terminal or 4-terminal geometry. For the former, whole pellets were sandwiched between two Cu disks using conducting Ag epoxy. For the latter, pellets were cut into ~7x3x3 mm bars and 4 separate Cu leads were attached using the same conducting epoxy.

3. Results and Discussion

Ceramic samples of $CaMn_{0.98}Nb_{0.02}O_3$ were synthesized using a standard solid state technique described in the experimental section. By preparing pellets of $CaMn_{0.98}Nb_{0.02}O_3$ with different concentrations of 6 μm diameter PMMA beads, the relative densities of the sintered samples were controlled accurately. The addition of between 1 and 10% w/w PMMA beads varied the relative density from 86 to 46%. A summary of the samples prepared is shown in Table 1. **Figure 2c** shows the variation in porosity as a function of PMMA bead

used during sintering. Interestingly, upon addition of a small percentage of PMMA beads the open porosity actually drops compared to the sample without PMMA and instead the majority of the pores are closed. Upon increase of PMMA beads the open porosity increases linearly and above 3% PMMA the open porosity exceeds that of the PMMA free sample.

SEM images of Samples G and H are shown in **Figures 2a** and **2b**, respectively. The large (18%) open porosity is evident in both samples as there are many interconnecting pore. This is particularly apparent when compared to Sample C, **Figure 2a inset**, where the closed porosity is much larger than the open. Clear regions of metallic Ag are evident in Sample H, however they are certainly not percolating throughout the sample and are only present in a small percentage of the visible pores. **Figure 2b inset** shows a higher magnification image of an Ag containing pore. Individual grains of ceramic are visible, roughly on the order of 5 – 10 μm diameter, and in some of the pores the Ag clearly coats these grains, although again the Ag pathways are not percolating and they appear to have agglomerated to an extent. EDX analysis on regions of Ag confirmed its presence. Smaller, sub-μm sized white spots are also visible in samples with and without Ag, however EDX analysis on these regions did not reveal any Ag. We believe this may be Nb segregation, as has been found in other Nb-doped oxide ceramics.[26] EDX analysis on regions of ceramic show only the presence of Ca, Mn, O and Nb, as expected. The Ca:Mn mass ratio lies between 67.5% and 71.2%, which is close to the 71.5% expected, whilst the Nb content is low (<5%) but more accurate determination of the latter was not possible with EDX. Whilst the images do not give a quantitative measure of the amount of Ag within infiltrated samples, it is clear that even in high porosity samples Ag does not enter every pore and only coats the grains of pores it does enter. Moreover, measurement of density before and after silver infiltration did not lead to any changes. Comparing these observations with the calculated maximum of Ag given the open porosity, shown in Table 1, these results indicate that the Ag loading using this technique is significantly less than the theoretical maximum.

We now turn to the thermoelectric properties of these samples. One aspect of this study was to examine whether significant improvement in inter-grain electrical conductivity of ceramics could be achieved through the infiltration of silver. A large reduction in electrical resistivity had been found in $La_{0.67}Ca_{0.33}MnO_3$ upon the addition of silver, which was interpreted as improvement in grain boundaries electrical connectivity.[27] Similar results have also been found in $Ca_3Co_4O_9$/Ag composites, whereby the improved electrical conductivity increases ZT with small amounts of Ag.[28-30] However, these studies focused only on 4-terminal electrical measurements, which removes the contact resistance and therefore does not reflect the performance characteristic of a working TEG.

The resistivity of our samples is shown in **Figure 3a**, plotted as a function of open porosity. It is immediately clear that all samples without Ag infiltration measured in 2-terminal geometry have resistivity at least 2 orders of magnitude larger than the same samples measured in 4-terminal geometry. Values measured in 4-terminal geometry are in good agreement with the literature and represent the intrinsic resistivity of the samples, although our measurements do not have the sensitivty to determine a systematic change with porosity. Values measured in 2-terminal geometry reveal the large contact resistance and, accordingly, this data should be considered an 'apparent resistivity'. However, upon addition of Ag the 2-terminal resistivity drops significantly for all samples and shows a decreasing trend with increased open porosity. Moreover, for large open porosity the resistivity drops below the intrinsic value of between $100 < \mu\Omega m < 400$ showing that silver starts to play a significant role.

Examination of the Seebeck coefficient and thermal conductivity taken together reveals further information on the effect of Ag infiltration. **Figure 3b** shows the Seebeck coefficient data. The data is not affected significantly when the measurement is taken in two terminal or four terminal geometry, from which we conclude that it is the bulk of the sample not the contacts that dominate the measurement. All samples without Ag have values between $-175 < S < -200$ μV/K, as expected for 2% Nb doped $CaMnO_3$, and show no noticeable trend with

porosity. With silver addition |S| decreases gradually with increased porosity to a value of -20 μV/K at ~50% open porosity. As Ag has a small, positive |*S*| (+2 μV/K) , the reduction in |*S*| is likely caused by short pathways of Ag contributing to the overall measurement. Fully connected percolating silver pathways would of course reduce the Seebeck coefficient to that of silver and it is seen to approach this value at 50% porosity, consistent with the dc resistivity results. At intermediate values of porosity, the material behaves as a composite structure. The addition of silver at the grain boundaries alone would not significantly affect *S* due to the additive thermoelectric voltages from the sample and Ag grains in series. Such behaviour has been found from the addition of Ag in other oxides.[31] Unlike the electrical transport, the thermal conductivity κ is a bulk measurement dominated by the thermal resistance bottlenecks and the data in **Figure 3c** shows no specific trend, although κ tends to decrease with increased porosity as would be expected. This supports the view of the sample as a composite structure with only a very small number of connecting silver pathways even at high porosity. The 4-terminal measurements of κ are likely giving a more accurate value, which in the literature is ~ 2.5 W m^{-1} K^{-1}.[4]

The thermoelectric power factor, PF = S^2/ρ, for samples measured in 2-terminal geometry is shown in **Figure 4a**. For samples without Ag infiltration the power factor is < 1 W m^{-1} K^{-2} because of the large resistivity. However, with Ag infiltration the power factor is > 10 W m^{-1} K^{-2} for all samples. With increasing open porosity, the power factor increases exponentially, peaks at ~ 150 W m^{-1} K^{-2} at 18% porosity, before decreasing exponentially again as the porosity increases further. This stems from the different trends in ρ and *S*. The former decreases nearly 2 orders of magnitude between 8 and 18% open porosity, however the latter only by 40%. Beyond 18% open porosity the relative change in ρ decreases whilst |S| continues to decrease further, thus causing a reduction in the power factor.

The behaviour of S^2/ρ is mirrored in ZT, **Figure 4b**, due to the negligible change in κ between samples. Ag infiltration in 2-terminal geometry leads to between a 2 and 4 order of magnitude increase in ZT. Moreover, for the same samples the peak ZT value of ~0.01,

compared to 0.025 found in 4-terminal geometry with no Ag, shows that essentially all of the thermoelectric power can be recovered in 2-terminal geometry through Ag infiltration. We could not find any reports of $CaMn_{0.98}Nb_{0.02}O_3$ being used in TEG modules, however a module including $Ca_{0.92}La_{0.08}MnO_3$ reported a ~33% performance decrease [32] and one using $Ca_{0.9}Nd_{0.1}MnO_3$ reported 80% performance decrease due to an internal resistance 490% larger than the theoretical.[22] In another oxide TEG consisting of NiO and $(Ba,Sr)PbO_3$, contact resistance causes a 43% drop in the achievable maximum power output.[33] Our results demonstrate that it may be possible to eliminate these losses in oxide TEGs through Ag infiltration. However, it is worth noting that TE materials with Ag infiltration may be limited by the mobility of Ag at high temperatures. Whilst high temperature thermoelectric measurements of our samples are required to determine the maximum operating temperatures, we note reports of continued operation of similar Ag infiltrated oxygen separation devices at 600°C.[34] Our results also raise the idea that 2-terminal performance may be improved via infiltration of other highly conducting materials, for instance carbon nanotubes or YSZ.[35, 36]

In conclusion, we have prepared $CaMn_{0.98}Nb_{0.02}O_3$ materials and investigated the role of open porosity and metallic Ag infiltration on their TE properties. We find that the TE properties of these oxides are reduced by several orders of magnitude when connected in 2-terminal geometry, but their promising properties are fully recovered through Ag infiltration. Our results open up the possibility of bridging the performance gap between the intrinsic TE and TEG device properties that have hindered the utilization of oxides as realistic TE materials.

Acknowledgements
The authors acknowledge funding from UK Funding body – the Engineering and Physical Sciences Research Council, Imperial College Impact Acceleration Account.

Table 1. List of samples prepared along with their relative densities and open porosities (OP) measured using the Archimedes method.

Sample	PMMA	Relative	Open	Silver?	Theoretical	Notes

	(w/w %)	Density (%)	Porosity (%)		maximum Ag (mg)	
A	0	86	8		14	
B	0	86	8	Y	14	
C	1	86	2		2	
D	1	86	2	Y	2	
E	3	82	10		17	
F	3	82	10	Y	17	
G	6	75	18		31	
H	6	76	18	Y	31	
I	10	68	29		50	
J	10	69	28	Y	49	
K	0	62	34		59	Not ball-milled
L	10	45	54		94	Not ball-milled

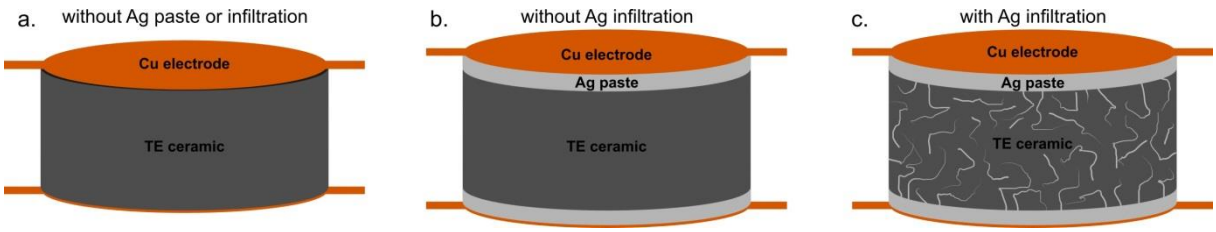

Figure 1. Schematic showing methods of improving contact resistances in a TEG module, from (a) a simple ceramic and electrode to (b) connection between the two with Ag paste to (c) metallic Ag infiltration in the TE ceramic. Ag infiltration is achieved using molten $AgNO_3$ which enters the pores of the ceramic pellets, created using PMMA pore former. The rapid cooling of the $AgNO_3$ allows it to remain within the pores. The nitrate is then decomposed to metallic Ag. The thermoelectric performance of samples without infiltrated Ag is several orders of magnitude smaller than with Ag due to large contact resistances.

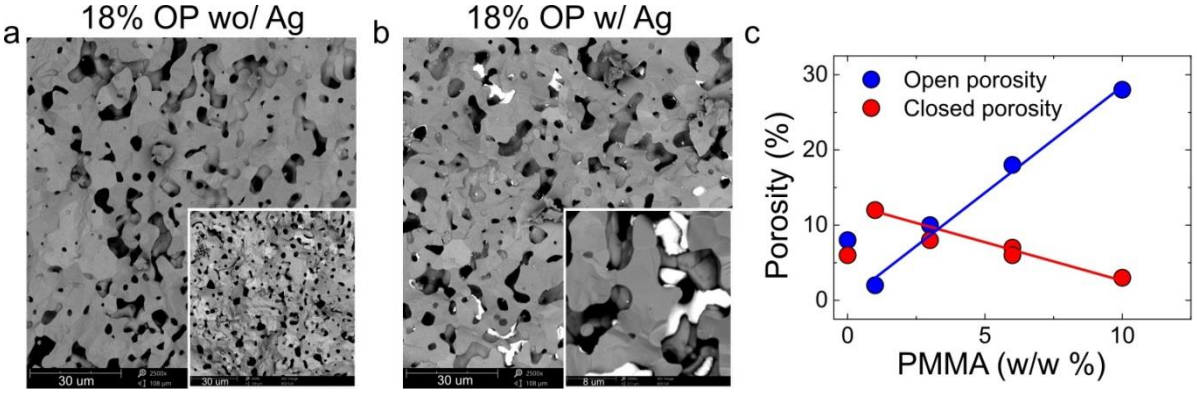

Figure 2. SEM images of Samples G (a) and H (b) without and with Ag infiltration, respectively, and both with 18% open porosity. The inset of (a) is of Sample C showing fewer interconnected pores. The inset of (b) is a higher magnification image of the same

sample in main figure (b) and shows the morphology of the silver. (c) Variation in open and closed porosity as a function of PMMA used during sintering.

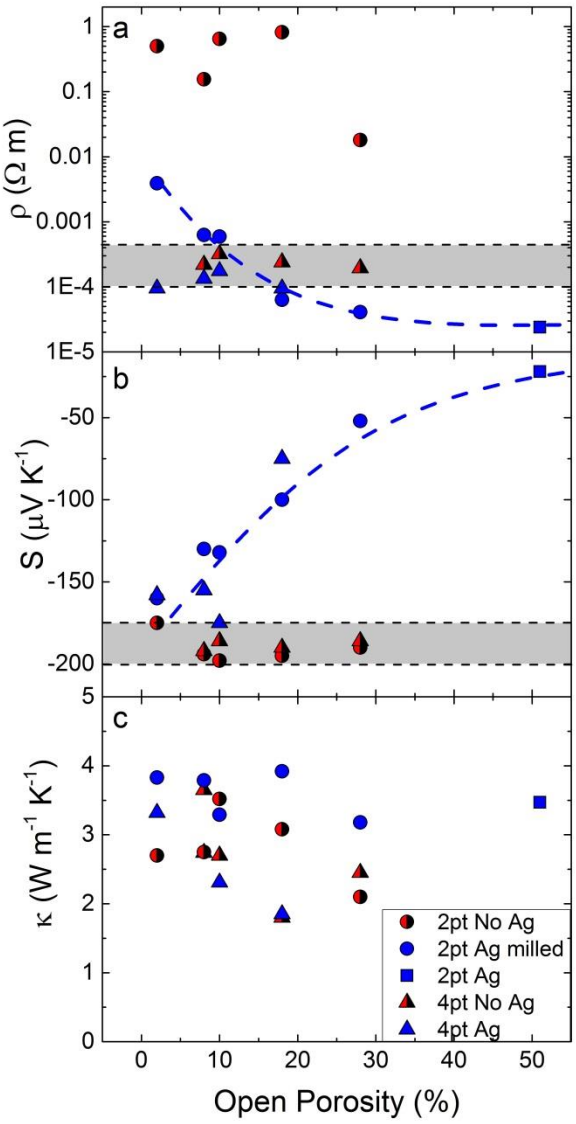

Figure 3. a. Electrical resistivity, b. Seebeck coefficient and c. thermal conductivity of $CaMn_{0.98}Nb_{0.02}O_3$ measured in 2- and 4-terminal geometry at 300K, with and without Ag infiltration. All data are plotted as a function of open porosity, which for the Ag infiltrated samples implies larger amounts of Ag. The grey bands in the ρ and S plots highlight the expected intrinsic value, thus showing in the former that ρ can be decreased upon the addition of Ag. The dashed lines in a and b are guides to the eye.

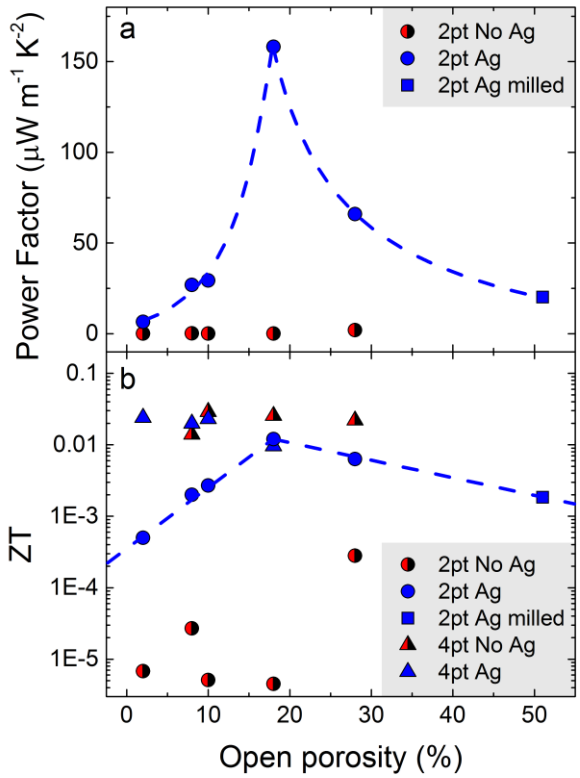

Figure 4. a. Thermoelectric power factor for 2-terminal measurements on samples with and without Ag infiltration. b. Thermoelectric figure-of-merit, ZT, for all samples. The dashed lines are guides to the eye.

[1] Venkatasubramanian, R., E. Siivola, T. Colpitts, B. O'Quinn, Thin-film thermoelectric devices with high room-temperature figures of merit, *Nature*, 413 (2001) 597-602.

[2] Zhao, L.-D., S.-H. Lo, Y. Zhang, H. Sun, G. Tan, C. Uher, C. Wolverton, D.V. P, M.G. Kanatzidis, Ultralow thermal conductivity and high figure of merit in SnSe crystals, *Nature*, 508 (2014) 373-377.

[3] Fergus, J.W., Oxide materials for high temperature thermoelectric energy conversion, *Journal of the European Ceramic Society*, 32 (2012) 525-540.

[4] Bocher, L., M.H. Aguirre, D. Logvinovich, A. Shkabko, R. Robert, M. Trottmann, A. Weidenkaff, CaMn1-xNbxO3 (x < 0.08) Perovskite-Type Phases As Promising New High-Temperature n -Type Thermoelectric Materials, *Inorganic chemistry*, 47 (2008) 8077-8085.

[5] Koumoto, K., Y. Wang, R. Zhang, A. Kosuga, R. Funahashi, Oxide thermoelectric materials: A nanostructuring approach, *Annual Review of Materials Science*, 40 (2010) 363-394.

[6] Kovalevsky, A.V., A.A. Yaremchenko, S. Populoh, P. Thiel, D.P. Fagg, A. Weidenkaff, J.R. Frade, Towards a high thermoelectric performance in rare-earth substituted SrTiO3: effects provided by strongly-reducing sintering conditions., *Physical chemistry chemical physics : PCCP*, 16 (2014) 26946-26954.

[7] Kovalevsky, A.V., A.A. Yaremchenko, S. Populoh, A. Weidenka, J.R. Frade, Effect of A-Site Cation Deficiency on the Thermoelectric Performance of Donor-Substituted Strontium Titanate, *Journal of Physical Chemistry C*, 118 (2014) 4596-4606.

[8] Snyder, G.J., E.S. Toberer, Complex thermoelectric materials, *Nature Materials*, 7 (2008) 105-114.

[9] Walia, S., S. Balendhran, H. Nili, S. Zhuiykov, G. Rosengarten, Q. Hua, M. Bhaskaran, S. Sriram, M.S. Strano, K. Kalantar-zadeh, Progress in Materials Science Transition metal oxides – Thermoelectric properties, *Progress in Materials Science*, 58 (2013) 1443-1489.

[10] Lu, Z., H. Zhang, W. Lei, D.C. Sinclair, I.M. Reaney, High-Figure-of-Merit Thermoelectric La-Doped A-Site-Deficient SrTiO3 Ceramics, *Chemistry of Materials*, 28 (2016) 925-935.

[11] Bocher, L., M.H. Aguirre, R. Robert, D. Logvinovich, S. Bakardjieva, J. Hejtmanek, A. Weidenkaff, High-temperature stability, structure and thermoelectric properties of CaMn1-xNbxO3CaMn1-xNbxO3 phases, *Acta Materialia*, 57 (2009) 5667-5680.

[12] Joshi, G., H. Lee, Y. Lan, X. Wang, G. Zhu, D. Wang, R.W. Gould, D.C. Cuff, M.Y. Tang, M.S. Dresselhaus, G. Chen, Z. Ren, Enhanced Thermoelectric Figure-of-Merit in Nanostructured p-type Silicon Germanium Bulk Alloys, *Nano Letters*, 8 (2008) 4670-4674.

[13] Snyder, G.J., T.S. Ursell, Thermoelectric Efficiency and Compatibility, *Physical Review Letters*, 91 (2003) 148301.

[14] Hung, L.T., N.V. Nong, S. Linderoth, N. Pryds, Segmentation of low-cost high efficiency oxide-based thermoelectric materials, *Physica Status Solidi A*, 212 (2015) 767-774.

[15] Noudem, J.G., S. Lemonnier, M. Prevel, E.S. Reddy, E. Guilmeau, C. Goupil, Thermoelectric ceramics for generators, *Journal of the European Ceramic Society*, 28 (2008) 41-48.

[16] Lippmann, W., M. Schreier, B.B. Feng, H.-p. Martin, B. Floriana-dana, K. Vogel, A. Lenk, I. Veremchuk, M. Dannowski, C. Richter, P. Pfeiffer, G. Zikoridse, H. Lichte, J. Grin, A. Hurtado, A. Michaelis, Manufacture and Testing of Thermoelectric Modules Consisting of BxC and TiOx Elements, *Advanced Engineering Materials*, 16 (2014) 1252-1263.

[17] El-Genk, M.S., H.H. Saber, High efficiency segmented thermoelectric unicouple for operation between 973 and 300 K, *Energy Conversion and Management*, 44 (2003) 1069-1088.

[18] Funahashi, R., S. Urata, Fabrication and Application of an Oxide Thermoelectric System, *International Journal of Applied Ceramic Technology*, 4 (2007) 297-307.

[19] Funahashi, R., S. Urata, K. Mizuno, T. Kouuchi, M. Mikami, Ca2.7Bi0.3Co4O9/La0.9Bi0.1NiO3 thermoelectric devices with high output power density, *Applied Physics Letters*, 85 (2004) 7-10.

[20] Hung, L.T., N.V. Nong, L. Han, R. Bjork, H. Ngan, T.C. Holgate, B. Balke, G.J. Snyder, S. Linderoth, N. Pryds, Segmented Thermoelectric Oxide-Based Module for High-Temperature Waste Heat Harvesting, *Energy Technology*, 3 (2015) 1143-1151.

[21] Hung, L.T., N. Van Nong, G.J. Snyder, M.H. Viet, B. Balke, L. Han, E. Stamate, S. Linderoth, N. Pryds, High performance p-type segmented leg of misfit-layered cobaltite and half-Heusler alloy, *Energy Conversion and Management*, 99 (2015) 20-27.

[22] Lim, C.H., S.M. Choi, W.S. Seo, H.H. Park, A power-generation test for oxide-based thermoelectric modules using p-type Ca3Co4O9 and n-type Ca0.9Nd0.1MnO3 legs, *Journal of Electronic Materials*, 41 (2012) 1247-1255.

[23] Ngan, P.H., N.G.O.V.A.N. Nong, L.E.T. Hung, B. Balke, L.I. Han, E. Marie, J. Hedegaard, S. Linderoth, N. Pryds, On the Challenges of Reducing Contact Resistances in Thermoelectric Generators Based on Half-Heusler Alloys, *Journal of Electronic Materials*, 45 (2016) 594-601.

[24] Seetawan, T., K. Singsoog, S. Srichai, C. Thanachayanont, V. Amornkitbamrung, P. Chindaprasirt, Thermoelectric Energy Conversion of p-Ca3Co4O9/n-CaMnO3 module, *Energy Procedia*, 61 (2014) 1067-1070.

[25] Teichert, S., A. Bochmann, T. Reimann, T. Schulz, C. Dreßler, J. Töpfer, S. Teichert, A. Bochmann, T. Reimann, T. Schulz, C. Dreßler, J. Töpfer, An oxide-based thermoelectric generator : Transversal thermoelectric strip-device, *AIP Advances*, 5 (2016) 077105.

[26] Sudireddy, B.R., P. Blennow, K.A. Nielsen, Microstructural and electrical characterization of Nb-doped SrTiO 3 – YSZ composites for solid oxide cell electrodes, *Solid State Ionics*, 216 (2012) 44-49.

[27] Turcaud, J.A., K. Morrison, A. Berenov, N.M. Alford, K.G. Sandeman, L.F. Cohen, Microstructural control and tuning of thermal conductivity in La0.67Ca0.33MnO3±δ, *Scripta Materialia*, 68 (2013) 510-513.

[28] Wang, Y., Y. Sui, J. Cheng, X. Wang, W. Su, Comparison of the high temperature thermoelectric properties for Ag-doped and Ag-added Ca3Co4O9, *Journal of Alloys and Compounds*, 477 (2009) 817-821.

[29] Wang, Y., Y. Sui, X. Wang, Efficient room temperature thermoelectric characteristics of Ca 3 − x Ag x Co 4 O 9 + δ / Ag y composites, *Journal of Physics D: Applied Physics*, 41 (2008) 045406.

[30] Wang, Y., Y. Sui, X. Wang, Efficient room temperature thermoelectric characteristics of Ca3−xAgxCo4O9+δ/Agy composites, *Journal of Physics D: Applied Physics*, 41 (2008) 045406.

[31] Mikami, M., N. Ando, R. Funahashi, The effect of Ag addition on electrical properties of the thermoelectric compound Ca3Co4O9, *Journal of Solid State Chemistry*, 178 (2005) 2186-2190.

[32] Matsubara, I., R. Funahashi, T. Takeuchi, S. Sodeoka, T. Shimizu, K. Ueno, I. Matsubara, R. Funahashi, T. Takeuchi, S. Sodeoka, Fabrication of an all-oxide thermoelectric power generator, *Applied Physics Letters*, 3627 (2001) 29-32.

[33] Shin, W., N. Murayama, K. Ikeda, S. Sago, Thermoelectric power generation using Li-doped NiO and (Ba,Sr) PbO3 module, *Journal of Power Sources*, 103 (2001) 80-85.

[34] Ruiz-Trejo, E., P. Boldrin, J.L. Medley-Hallam, J. Darr, A. Atkinson, N.P. Brandon, Partial oxidation of methane using silver/gadolinia-doped ceria composite membranes, *Chemical Engineering Science*, 127 (2015) 269-275.

[35] Wang, N., H. Chen, H. He, W. Norimatsu, M. Kusunoki, K. Koumoto, Enhanced thermoelectric performance of Nb-doped SrTiO3 by nano-inclusion with low thermal conductivity., *Scientific reports*, 3 (2013) 3449.

[36] Zhang, S., A. Li, K. Sun, X. Sun, S. Wang, Z. Liu, Thermoelectric properties of CNTs/Mn0.7Zn0.3Fe2O4 composite fabricated by spark plasma sintering, *Materials Research Express*, 3 (2016) 106303.